Effects of Various Re-Entry Vehicle Parameters on Radio Frequency Attenuation

F. A. VICENTE*
Aerospace Corporation, El Segundo, Calif.

The effects of antenna location, cone angle, nose radius, signal frequency, vehicle velocity, and wall temperature on rf signal attenuation are examined. For the assumptions of a clean air equilibrium flow and a thin slab electromagnetic model, the results indicate that a great reduction in rf signal attenuation can be achieved by proper aerodynamic shaping of the vehicle. Sample calculations are made for a transmission frequency of 600 mc for nose bluntness varying from $\frac{1}{4}$-in. to 1-ft radius, cone angles from 10° to 60°, wall enthalpies from 300 to 1200 Btu/lb, and velocities from 20,000 to 24,000 fps for a range of altitudes of 50,000 to 200,000 ft. Altitude-velocity maps for lines of constant attenuation are also presented. Results indicate that, for sharp slender bodies, rf attenuation can be limited to 10 db throughout the re-entry envelope.

Nomenclature

a = speed of sound
C_0 = speed of light in a vacuum
db = attenuation
dS/dn = entropy gradient normal to streamline
e = charge
E = electric field
f_t = transmission frequency, cps
g = mass conversion factor, 32.2 lbm/slug
h_i = enthalpy
h_w = wall enthalpy
J = energy conversion factor, 778 ft-lb/Btu
J = current density
L = plasma thickness
m = electron mass
N = number density of electrons
n_0 = $\omega/C_0 = 2\pi/\lambda_0$
R_i = radius of curvature in the hodograph plane
R_n = nose radius
S = specific entropy
T = transmission coefficient
u = velocity component in axial direction
v = velocity component in radial direction
v = electron drift velocity
v_{ni} = velocity normal to ray
v_{ri} = velocity along ray
V = freestream velocity
V_e = re-entry velocity, kft/sec
V_{lim} = limiting velocity
W = V/V_{lim}
X = $(\omega_p/\omega)^2$
γ = ratio of specific heats
$\Delta\theta$ = angular increment from ray to ray
η_e = electron density, electrons/cm^3
θ = flow angle
θ_c = cone half angle, deg
λ_0 = free space wavelength
μ = Mach angle
ψ = stream function
ω = transmission frequency, rad/sec
ω_c = collision frequency, collision/sec
ω_p = plasma frequency, rad/sec

Introduction

ALTHOUGH the use of aerodynamic shaping has been considered a solution to the rf attenuation problem, the importance of various vehicle parameters on signal fade has not received sufficient detailed attention. It is the purpose of this paper to examine the effect of: 1) antenna location; 2) cone angle; 3) nose bluntness; 4) signal frequency; 5) vehicle velocity; and 6) wall temperature, for a sphere-cone configuration. These effects are examined in detail in order to provide a logical basis for identifying those shaping parameters that most effectively reduce rf signal attenuation.

Although heat-shield materials appear to represent a large contribution to rf attenuation by the injection of various impurities into the flow streaming over the antennas, this report does not consider the effect of impurities. Obviously, with the vast number of heat-shield materials available and with the varying range of impurities which these materials contain from sample to sample, it becomes an impossible task to examine impurity effects for a parametric study of the type attempted here. It is possible, however, to examine all other parameters that have an important effect on signal loss by using clean air, and thereby to show the trends that are present rather than the actual absolute values of attenuation. As may be noted, vehicle attitude (angle of attack) effects are also not presented. However, it is possible to obtain an indication of attitude angle effects simply by the use of the cone-angle results presented. Although angle of attack may not, in a strict sense, be superimposed on the cone angle, such a superposition can lead to valid qualitative results.

Additional Assumptions

The prediction of rf attenuation during re-entry involves analysis of: 1) the flow field around the vehicle; 2) the chemical kinetics of the air; and 3) the electromagnetic effects due to the presence of an electric field induced by the antennas.[1] These disciplines are mutually coupled, but, as a first approximation, they are considered as separate entities and analyzed individually.

Because this paper is restricted to sphere-cone vehicles at zero angle of attack, it is possible to analyze the inviscid flow about a vehicle that has a specified degree of nose bluntness by the method of characteristics for axisymmetric rotational flow.[2] For a relatively sharp-nosed slender body, which has a turbulent boundary layer, conical flow methods may be used to analyze regions greater than 40 nose radii downstream of the nose. Therefore, for most sharp-nosed vehicles and for blunt-nosed vehicles where it is not possible to place antennas forward of the 40 nose-radii station, the analysis of the flow field in the vicinity of the antennas can be based on a sharp cone with an attached shock. With the inviscid flow field established, the usual treatment of the viscous boundary layer is possible. Laminar and turbulent

Received February 27, 1964; revision received June 16, 1964.
* Member of Technical Staff.

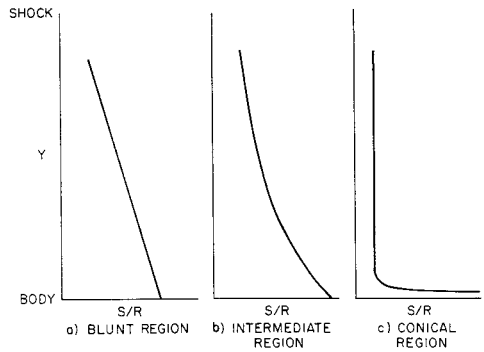

Fig. 1 Entropy distribution normal to vehicle wall.

flow may be considered and the required plasma parameters computed.

The dissociation and ionization problem can be bounded by considering a frozen and an equilibrium air state. For sharp-nosed bodies ($R \leq \frac{1}{2}$ in.), equilibrium flow predominates at altitudes lower than 125,000 ft, but nonequilibrium dissociation effects are important for higher altitudes. Recent work[3] has established the rates at which these nonequilibrium dissociation reactions proceed. However, for sharp-nosed, slender bodies, dissociation and ionization effects are localized to the nose tip and the thin boundary-layer region. Consequently, since 1) the effect of contaminants in the boundary layer (e.g., from heat shields) is difficult to establish for a general study of the type attempted here; 2) the altitude, where an overdense plasma is expected, is on the order of 100,000 ft; and 3) the purpose of this paper is to show trends rather than absolute values, the chemical kinetic approach selected for this study is equilibrium chemistry for clean air.

The presence of an overdense plasma in the vicinity of an antenna causes three phenomena that have an adverse effect on rf signals. These phenomena are: 1) attenuation of the rf signal due to electromagnetic interaction with the electrons in the plasma; 2) antenna pattern distortion due to the presence of the plasma; and 3) antenna breakdown, which can occur at lower power levels than in the no plasma case. Only the electromagnetic interaction effects are presented here, using primarily the thin plasma slab model of Gold.[4] Because much earlier work has been performed, using a semi-infinite model, constant attenuation lines are presented using both methods, but the thin-slab model more closely resembles the actual physical case and should more nearly agree with the experimental flight attenuation results.

Because antenna pattern distortion due to the presence of a plasma is extremely difficult to measure under actual flight conditions, a nondistorted pattern is usually assumed in the reduction of flight data. Some portion of the observed signal loss could be attributed to pattern distortion rather than to rf attenuation, but since the actual magnitude of this effect has not been established, it is neglected herein. Antenna breakdown is well defined for a low-pressure environment; although the presence of plasma would be expected to change the properties causing antenna breakdown, it is not considered significant at low telemetry levels and will be neglected for this study.

Method of Analysis

The region in the vicinity of the nose is governed by flow effects that arise as a result of the air passing through a strong curved shock. At some distance far from the nose, the shock reaches the limiting conical value. (The greater the bluntness, the farther rearward will conical flow be established.) Little or no ionization should be present in this inviscid conical region because of the relatively low temperatures involved. The highly rotational flow produced by the strong shock region remains in a narrow layer close to the body and is eventually completely swallowed by the boundary layer, so that the inviscid portion of the flow field appears to behave essentially like a conical flow as far as attenuation is concerned.

In order to be able to compute the flow properties in this region, the numerical method of characteristics must be used. Fortunately, such a solution for an axisymmetric flow is available and is used in this paper. However, a severe limitation exists in the use of the method of characteristics in computing the inviscid flow field continuously from the blunt region to the fully conical region. This limitation arises from the usual assumption of constant entropy gradient along the characteristic lines.

In order to solve the usual nonlinear partial differential flow equation for axisymmetric flow, Ref. 5 gives the following expression:

$$[1 - (u/a)^2]\psi_{xx} - 2(uw/a^2)\psi_{yx} + [1 - (v/a)^2]\psi_{yy} - \psi_y/y - y^2(1 - W^2)^{(\gamma+1)/(\gamma-1)}(W^2/a^2 - 1)f(\psi) = 0$$

Two compatibility relations arise; namely, for characteristics of the first family,

$$\frac{dW}{W} - \tan\mu\, d\theta - \frac{dx}{y}\frac{\sin\mu\,\tan\mu\,\sin\theta}{\cos(\theta + \mu)} + \frac{dS}{dn}\frac{dx}{g\gamma R}\frac{\sin^3\mu}{\cos(\theta + \mu)} = 0$$

and for characteristics of the second family,

$$\frac{dW}{W} + \tan\mu\, d\theta - \frac{dx}{y}\frac{\sin\mu\,\tan\mu\,\sin\theta}{\cos(\theta - \mu)} - \frac{dS}{dn}\frac{dx}{g\gamma R}\frac{\sin^3\mu}{\cos(\theta - \mu)} = 0$$

The intersection of the characteristics is governed by $dy/dx = \tan(\theta + \mu)$ for the first family and $dy/dx = \tan(\theta - \mu)$ for the second family.

It is observed that the compatibility equations form a system of two equations having three unknowns, dW, $d\theta$, and dS. Ferri[5] makes the perfectly valid assumption of constant entropy gradient along the characteristics; this assumption is valid not only for flows with constant entropy gradient but also for flows where a very gradually changing entropy gradient exists. In the latter case, a fine mesh size will yield valid results. However, if the calculation is made over an entire slender body, the entropy distributions noted in Fig. 1 would be expected.

As seen from Fig. 1c, a very sharp elbow exists in the entropy distribution, and, consequently, an extremely fine mesh size would be required to permit a valid solution. If such a mesh size were used, two events would occur, namely, 1) an increase in numerical errors due to the many more calculations per unit length, and 2) a tremendous increase in machine computing time.

However, by carrying the computation to the intermediate stage and then graphically patching this to a conical solution, which is assumed to exist at infinity, a small error is introduced, but satisfactory results may be obtained. Conical flow fields may be solved rather easily by the use of the hodograph plane to set up the difference relations required.[5] By proper recasting of the equations to include real-gas effects and by using an iterative approach that uses the shock as the starting point, results identical to those of Romig[6] may be obtained. The expressions used are as follows:

$$R_i = [-v_{n_i}\cot\theta_i - v_{r_i}]/[1 - (v_{n_i}/a_i)^2]$$

$$v_{n_{i+1}} = v_{n_i}\cos\Delta\theta - (R_i - v_{r_i})\sin\Delta\theta$$

$$v_{r_{i+1}} = -v_{n_i}\sin\Delta\theta - (R_i - v_{r_i})\cos\Delta\theta + R_i$$

$$h_{i+1} = h_{\text{stag}} - (v_{n_{i+1}}{}^2 + v_{r_{i+1}}{}^2)/2gJ$$

The laminar boundary layer is computed by the method of Van Driest[7] and for turbulent flow the method of Walker[8] is used. References 9 and 10 yield the thermodynamic properties and the electron densities present in the flow, respectively. The collision frequency between electrons and molecules is found by the method described by Musal.[11] Reference 4 can then be used to compute the rf attenuation once the plasma parameters have been determined. The conductivity function that characterizes the electromagnetic properties of an ionized gas can be determined from the equation of motion of an electron, namely,

$$m d\mathbf{v}/dt + m\omega_c \mathbf{v} = e\mathbf{E}$$

A plane electromagnetic wave is assumed to impinge in the normal direction to a plasma slab varying in thickness $0 < z < L$. The plasma properties are assumed to vary in the z direction only, thereby allowing an inhomogeneous electron distribution to be considered which is the case physically. With these conditions and the relation $\mathbf{J} = Ne\mathbf{v}$, the preceding differential equation may be solved for the current density and then substituted into Maxwell's equations to yield

$$F_j'' + n_0^2(1 - kX_{(z)})F_j = 0$$

$$G_j = -F_j'/n_0$$

where $j = 1, 2$, for the right- and left-handed circularly polarized waves, respectively, and $k = 1 - i\omega_c/\omega$.

For the limiting case, which is appropriate here because of the thin boundary-layer plasma, i.e., $L/\lambda_0 \ll 1$, the function $X_{(z)}$ is represented by a Dirac delta function at $z = 0$, $\delta_{(z)}$,

$$X_{(z)} = (\bar{X}L)\delta_{(z)}$$

where

$$\bar{X}L = \int_0^L X_{(z)} dz$$

Substituting into the second-order differential equation, and integrating once from 0 to z,

$$F_j' = (F_j')_0 + n_0^2 k\bar{X}L(F_j)_0$$

which leads to

$$T = 1/(1 - in_0 k\bar{X}L/2)$$

When the Poynting vector is evaluated

$$\epsilon_T = (T)^2$$

then the attenuation is

$$\text{db} = 10 \log_{10}\epsilon_T$$

The assumption that the transmission across a thin inhomogeneous plasma sheath depends on the integrated value of electron density and not on the detailed distribution has been shown to introduce only a slight error into the calculation.[4]

For a semi-infinite plasma model, the analysis of Rheinstein[12] could be used, but for the sharp slender bodies analyzed here, the attenuation due to reflection alone is important; hence, the absorption portion of the semi-infinite model may be neglected.

Results

The results are grouped in such a way that electron densities and attenuation values appear together for each parameter analyzed. The parametric effects presented are: 1) antenna location; 2) cone half-angle; 3) variation of transmission frequency; 4) nose radius; 5) vehicle velocity; and 6) wall temperature. The attenuation values presented are for a transmission frequency of 600 Mc, which was chosen because it represents a median in the range where the variation of attenuation with frequency is small. Figure 2a shows a typical variation of maximum electron density along the length of the body. Figure 2b shows values of attenuation as a function of vehicle body station for a wall enthalpy of 300 Btu/lb. Figure 3 shows a typical profile of electron density within the boundary layer. This distribution of electron density was obtained, as were all the other results in this paper, assuming a turbulent boundary layer. Figure 4 shows the same parameters as Fig. 2 but for 1200 Btu/lb. As observed from these figures, the maximum electron density essentially reaches the conical flow value at $x/R_n \geq 35$ for all cone angles, but the level of attenuation at any x/R_n is a pronounced function of cone angle. For cone angles below 30°, the conical-flow value of attenuation is reached at lesser values of x/R_n. For high cone angles ($\theta_c > 30°$), a minimum attenuation exists near $x/R_n = 5$, because the boundary layer is relatively thin in this region, but, for the conical portion of the flow field, the flow behaves as expected and a higher cone angle yields a higher attenuation. However, the minimum-attenuation "window" is not easily used because its location varies with altitude and because it occurs so close to the nose. For these results, it can be inferred, for example, that antennas located 10 or more inches behind a $\frac{1}{4}$-in. nose should give minimum attenuation; this

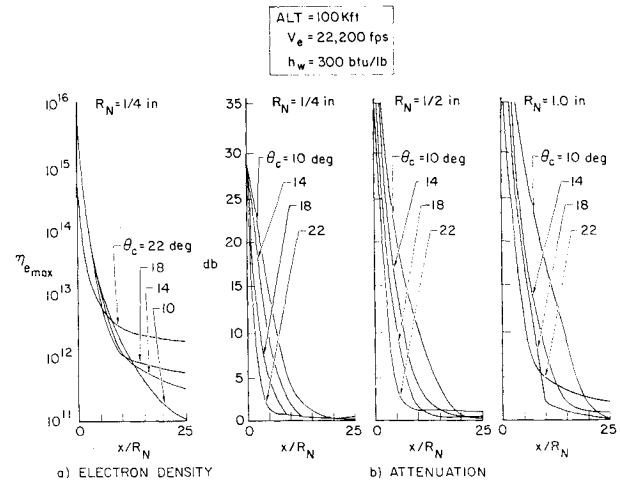

Fig. 2 Longitudinal variation of electron density and rf attenuation for h_w = 300 Btu/lb.

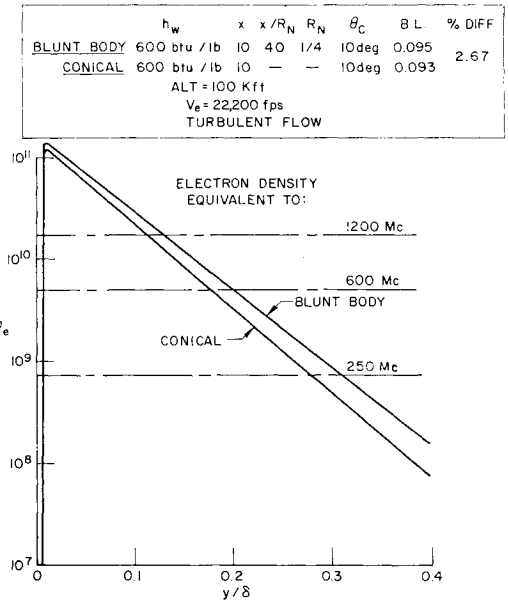

Fig. 3 Typical boundary-layer electron density profile

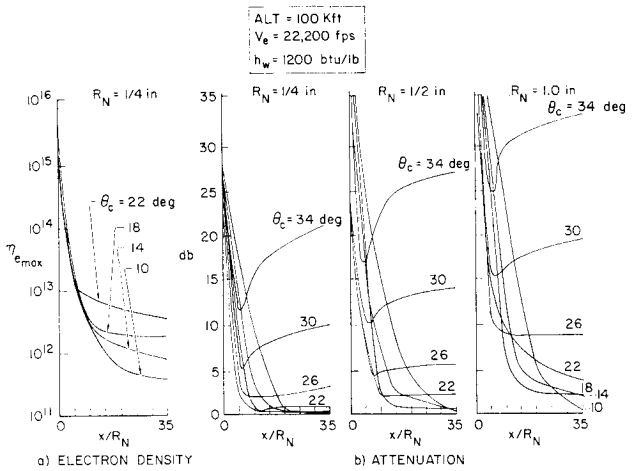

Fig. 4 Longitudinal variation of electron density and rf attenuation for h_w = 1200 Btu/lb.

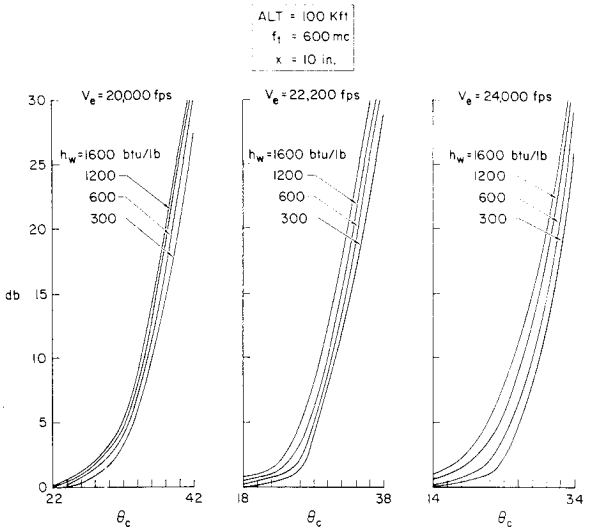

Fig. 6 Variation of attenuation vs cone angle.

inference is, of course, valid only for altitudes less than 125,000 ft.

Figure 5a shows the variation of electron density with cone angle for the inviscid flow. It indicates that no electron contribution to rf attenuation from the inviscid layer, which would affect VHF or UHF transmission, is expected for $\theta_c < 20°$ at altitudes below 200,000 ft. Consequently, for all practical cases of slender bodies, the boundary layer is the sole contributor to rf attenuation. This greatly simplifies the analysis, because the inviscid calculations may be limited to those which provide inputs to the boundary-layer calculation. For frequencies above 35 gigacycles (Gc), the contribution of the inviscid region of rf attenuation is limited to angles above 28° to 34°. The stagnation region is shown to be a contributor for all cases where equilibrium flow is expected. For transmission frequencies of 250 Mc to 35 Gc, the contribution of the inviscid layer depends primarily on the thickness of the layer.

The contribution of the boundary layer can be seen immediately from Figs. 5b and 5c. It will be noticed that the electron densities are above equivalent VHF frequencies for all cone angles at altitudes below 200,000 ft for the velocity examined. Figure 6 indicates that the contribution of electrons to the rf attenuation becomes strong for angles in excess of 30°. In particular, the attenuation for low cone

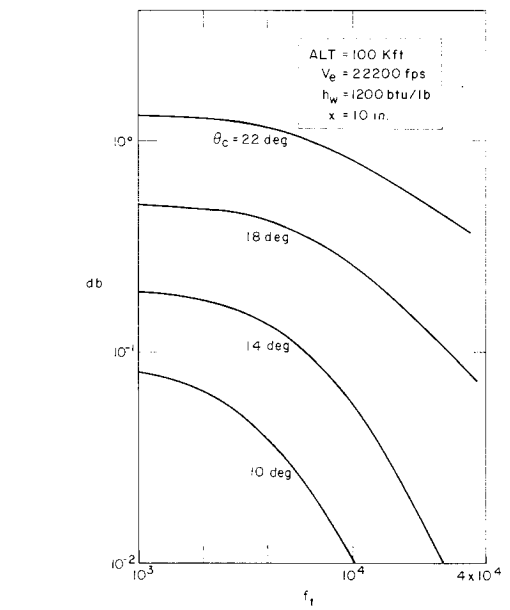

Fig. 7 Typical variation of rf attenuation as a function of transmission frequency.

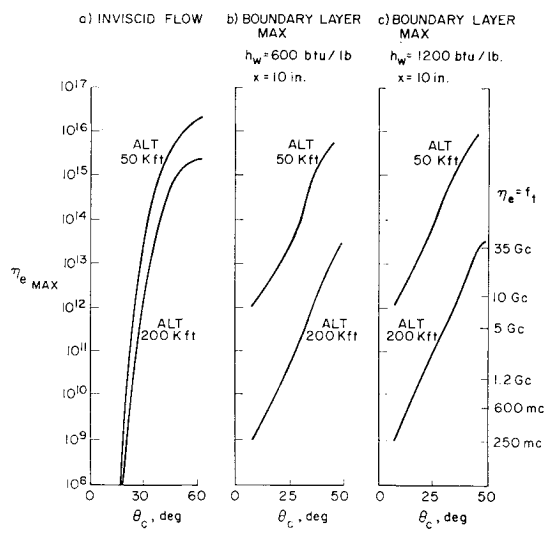

Fig. 5 Variation of maximum electron density vs cone angle.

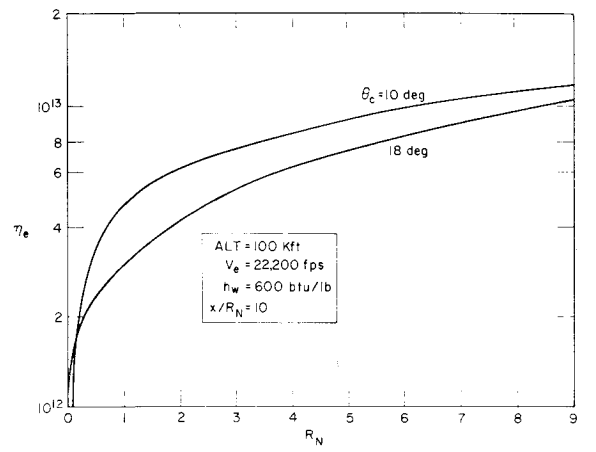

Fig. 8 Variation of electron density vs nose radius.

angles is observed to be very small. The temptation is to say that the flow of clean air over bodies with low cone angles contributes very little to the attenuation of an rf signal. A word of caution should be interjected here inasmuch as the electromagnetic equations assume a plane wave, impinging on the plasma. In most real instances, the plasma

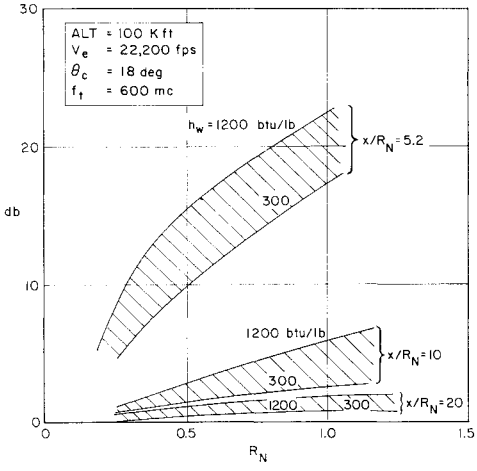

Fig. 9 Variation of attenuation for sharp-nosed vehicles.

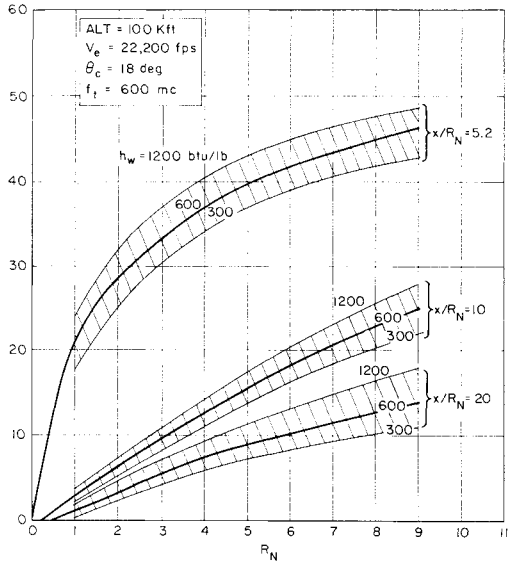

Fig. 10 Variation of attenuation for blunt-nosed vehicles.

is in the near field of the antenna where the interaction is not well understood, and, consequently, all that can be deduced from these figures is trends. The trends, as indicated by both the variation of electron density and the attenuation with antenna location and cone angle, are consistent, but the actual magnitude of attenuation for slender bodies must be provided by experiment.

Figure 7 presents a typical representation of the influence on attenuation of the transmission frequency; this figure indicates that the attenuation remains constant well into the gigacycle range. In particular, the attenuation changes very little until the frequency has increased over 5 Gc. This effect appears regardless of which theory is used, i.e., either the finite thin slab or the semi-infinite plasma theory.

Figure 8 indicates that a reduction of nose radius from 1 ft to 1 in. reduces the electron density by approximately a factor of three. A further reduction to 0.1 in. reduces the concentration by a total factor of 10; a similar reduction can be achieved by reducing the cone angle by an increment of 10°. These two reductions should be considered as additive in terms of attenuation reduction. Corresponding attenuations for three different body stations at three different wall

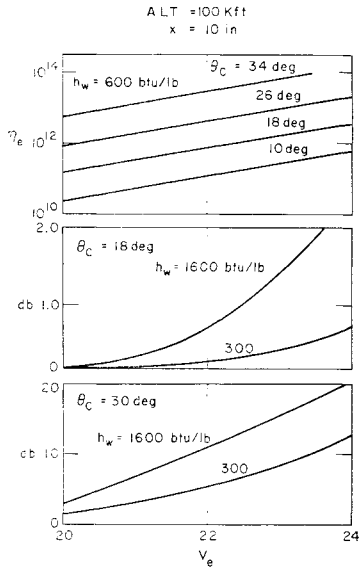

Fig. 11 Typical variation of electron density and rf attenuation vs velocity.

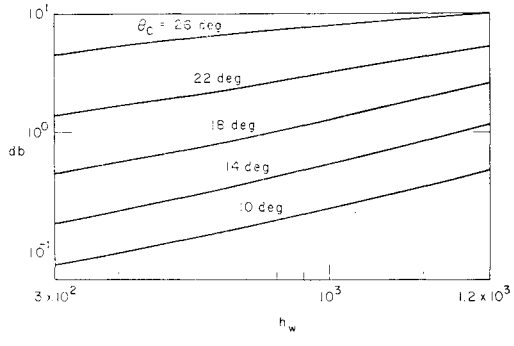

Fig. 12 Dependence of attenuation on wall enthalpy.

temperatures, given in Figs. 9 and 10, indicate that the largest drop in attenuation is achieved when the nose radius is reduced from 1 to 0.1 in. Consequently, the advantage that is gained from reducing the tip diameter is to move the flow disturbance further forward toward the stagnation region producing a lower signal attenuation further forward on the body.

An order of magnitude drop in the electron density is achieved by reducing the velocity by 3000 fps, as observed from Fig. 11. This results in a marked drop in attenuation due to the strong dependence of ionization on kinetic energy.

The effects of wall temperature can be expressed in terms of the value of enthalpy at the wall. A drop of 600 Btu/lb decreases the electron density by a factor of 2 to 3, resulting in a marked decrease in attenuation. From Fig. 12 it is observed that a drop in enthalpy of 600 Btu/lb is equivalent to reducing the cone angle by 4°.

Lines of constant attenuation for a 600 Mc transmission frequency (Fig. 13) indicate a weak altitude dependence of attenuation for the limiting case of orbital re-entry (approximately 26,000 fps). Table 1 may be generated as a quick determination of the lowest boundary of signal loss. In actual flight conditions, the attenuation will be higher due to the chemical kinetic and electromagnetic effects.

Table 1 Cone angle vs attenuation

θ_c, deg	db loss
10	1.0
14	3.0
18	6.0
22	11.0

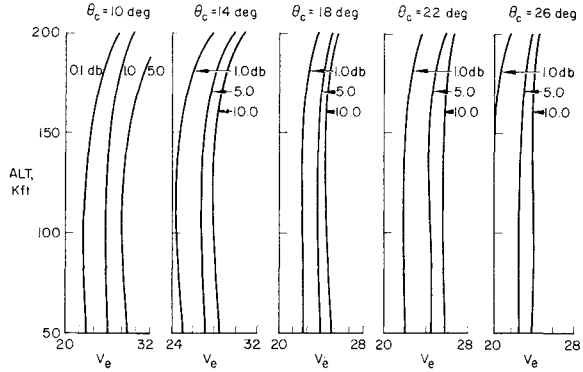

Fig. 13 Altitude-velocity map of lines of constant rf attenuation (thin slab).

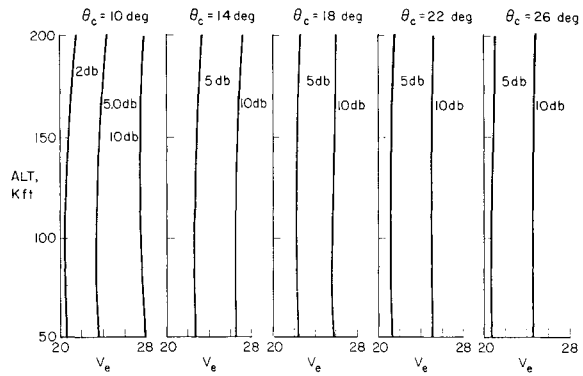

Fig. 14 Altitude-velocity map of lines of constant rf attenuation (semi-infinite).

Figure 14 represents the same calculation as in Fig. 13 except that the semi-infinite slab model is used. It is noticed that up to an angle of 22° a large discrepancy occurs between the two theories. However, for a cone angle of 26°, similar results are obtained because in the semi-infinite case, only the attenuation due to reflection is examined (absorption is neglected), whereas in the finite slab case, the attenuation is a function of thickness.

Conclusion

This paper has examined the effects of antenna location, cone angle, nose radius, signal frequency, vehicle velocity, and wall temperature on rf signal attenuation. Individually the conclusions drawn are as follows:

1) For minimum attenuation, this study indicates that antennas should be placed well back from the nose region.

2) A sharp slender body with a cone angle less than 20° restricts the ionization region to the boundary layer, and no appreciable attenuation is found for cone angles less than 20°.

3) The decrease in attenuation due to an increase in transmission frequency is significant only for transmission frequencies in excess of 5 Gc.

4) A sharp pointed nose ($R_n < \frac{1}{2}$) limits the blunt-body attenuation effects to $x/R_n < 35$.

5) A small decrease in velocity infers a large decrease in attenuation.

6) A 600 Btu/lb decrease in wall enthalpy is equivalent to reducing the cone angle by 4°.

From the results presented, it is observed that a great reduction in signal attenuation can be achieved by combining various parameters, for example, by locating the antennas sufficiently rearward, decreasing the cone angle to below 20°, insuring that the vehicle retains a sharp pointed nose radius (less than $\frac{1}{2}$ in.) throughout the region where transmission is required, and using a clean ablator that provides a relatively cold wall to the flow. It is recognized that a particular application may not permit all these reductions to be achieved. However, it is still possible to achieve significant reductions by making use of the individual favorable conditions outlined in this paper.

References

[1] Vicente, F. A., "Approximate calculation of rf attenuation for a lifting re-entry vehicle," Aerospace Corp. TDR-169 (3116-40) TN-2 (June 1963).

[2] Vaglio-Laurin, R. and Trella, M., "A study of flow fields about some typical blunt-nosed slender bodies," Polytechnic Institute of Brooklyn, Rept. 623 (December 1960).

[3] Wray, K. L., "Chemical kinetics of high temperature air," ARS Paper 1975-61 (August 1961).

[4] Gold, R. R., "Reflection and transmission of electromagnetic waves from inhomogeneous magneto-active plasma slabs," Aerospace Corp. TDR-169 (3230-11) TN-12 (March 1962).

[5] Ferri, A., *Elements of Aerodynamics of Supersonic Flows* (Macmillan Co., New York, 1949), Chaps. 12, 13.

[6] Romig, M. F., "Conical flow parameters for air in dissociation equilibrium," Convair RR 7 (1960).

[7] Van Driest, E. R., "Investigation of laminar boundary layer in compressible fluids using the Crocco method," NACA TN2597 (January 1952).

[8] Walker, G. K. and Schuman, B. A., "The growth of turbulent boundary layers," General Electric Co., Missile and Space Vehicle Div., TIS R61SD123 (July 1961).

[9] Moeckel, W. E. and Weston, K., "Composition and thermodynamic properties of air in chemical equilibrium," NACA TN4265 (April 1958).

[10] Feldman, S., "Trails of axisymmetric hypersonic blunt bodies flying through the atmosphere," AVCO RR 82 (December 1959).

[11] Musal, H., Jr., "Electron collision frequency in equilibrium high temperature air," Bendix Products Div., Advanced Development Labs., Bendix Aviation Corp., RN-9 (May 1960).

[12] Rheinstein, J., "Curves of transmission and reflection of an electromagnetic wave by a plane, uniform plasma slab," Lincoln Lab. Rept. PA-6* (March 1962).